Energy Aware Trajectory Optimization of Solar Powered AUVs for Optical Underwater Sensor Networks

Khadijeh Ali Mahmoodi, *Student Member, IEEE,* Murat Uysal, *Fellow, IEEE*

***Abstract*—Visible light communication (VLC) provides an alternative underwater wireless connectivity solution with its low latency and high data rates albeit at relatively shorter distances in the order of tens of meters. In the context of underwater sensor networks (USNs), VLC is particularly suitable to establish connectivity between "data mule" autonomous underwater vehicles (AUVs) and sensor nodes since communications is enabled only when the sensor node and mule AUV are in close proximity. In this paper, we consider a USN scenario where a solar-powered AUV gathers data from the sensor nodes using VLC signaling. We formulate a three-dimensional trajectory optimization for solar-powered AUVs with the goal of maximizing the harvested energy under constraints imposed by the data transmission. The optimization constraints include the minimum required data transfer rate, therefore a corresponding transmission distance, between the sensors and the AUV. We formulate the problem as a bilevel optimization problem. The lower-level objective function is in the form of traveling salesman problem which determines the optimum sequence order of the sensor nodes to be visited while the upper-level objective function is the optimization of the trajectory between each pair of adjacent nodes for the given order of node visits. Our numerical results demonstrate that the proposed trajectory significantly prolongs the mission time and autonomous operation of the AUV without the need to return to home base. Furthermore, since the proposed trajectory optimization is reactive to ocean currents, it brings reductions in the energy consumption of the AUVs.**

***Index Terms*—Visible light communication, underwater sensor networks, trajectory optimization.**

I. Introduction

Underwater sensor networks (USNs) have been increasingly deployed in various maritime applications including pollution monitoring, tsunami warnings, underwater oil field detection, and valuable minerals explorations among others [1]. Conventional USNs typically involve static sensor nodes distributed in a large-scale marine environment. After the sensor data is collected at a gateway node, e.g., a buoy or support vessel, it can be transmitted to a remote location via wireless or optical links [2]–[5]. Based on the distance between underwater sensor nodes and the gateway node, underwater data collection can be made either via a single hop or multiple hops. The multi-hop transmission has the problem of unbalanced energy consumption., e.g., sensors that are close to the gateway node deplete their energies faster, leading to what is known as "energy holes" [6] around the gate node. Furthermore, individual node failures may result in disruption or degradation of the end-to-end communication.

This work has been funded by the European Union's Horizon 2020 research and innovation program under the Marie Skłodowska Curie grant agreement ENLIGHTEM No. 814215.

Kh. Ali Mahmoodi and M. Uysal are with the Department of Electrical and Electronics Engineering, Özyeğin University, 34794 Istanbul, Turkey (e-mail: Khadijeh.ali@ozu.edu.tr; murat.uysal@ozyegin.edu.tr).

The increasing adoption of autonomous underwater vehicles (AUVs) provides novel approaches to tackle underwater data collection in USNs. For example, AUVs can be efficiently deployed as "data mules" to retrieve data from sensor nodes via a wireless link [7]. In an AUV-assisted USN, AUV travels around and gathers data from static sensor nodes. This helps decrease the energy consumption of sensor nodes since they are no longer responsible for data relaying and routing to transfer the aggregated data to the gateway node [8]. The required energy of the sensor nodes to send their own data is also reduced due to shorter transmission distance.

For underwater wireless transmission, acoustic signaling is commonly used and particularly appealing with its long range in the order of kilometers [9]. However, acoustic communication suffers from low data rates (in the order of tens of kb/s) and low propagation speed (1500 m/s) [8]. An alternative underwater wireless connectivity solution is visible light communication (VLC) offering low latency and high data rates in the order of Gb/s, albeit at relatively shorter distances (in the order of tens of meters) [10]. VLC is particularly suitable for data mule AUVs since communications is enabled only when the sensor node and mule AUV are in close proximity. Underwater VLC systems can be implemented using either light emitting diodes (LEDs) or laser diodes (LDs) as wireless transmitters [11]–[13]. LED-based underwater VLC systems provide lower data rates as compared to LD-based counterparts, however are more robust to pointing errors.

In this paper, we consider a USN scenario where an AUV gathers data from the sensor nodes using VLC signaling. While such an AUV-assisted USN offers significant advantages in network operations such as data collection and localization, the introduction of mobile nodes presents challenges such as sophisticated trajectory planning and energy-efficient operation of AUVs whose mission time are mainly limited with battery capacity. Energy consumption is also related to the type of deployed AUVs. Propelled AUVs can reach higher speeds, but their power consumption can be large due to the continuous use of propeller engine [14]. In contrary, non-propelled AUVs (gliders) use little to no power, but operate at much lower speeds [15]. Floating up and diving in operations in non-propelled AUVs is also possible by changing their buoyancy with little power consumption [16]. Hybrid versions [17] use their buoyancy engine for floating up and diving and use their propeller engine for going forward. In the operation of AUVs, the main power consumption source is therefore propeller engine. The choice of trajectories therefore directly impacts the mission time and energy consumption.

Since the energy efficiency of predefined trajectories [18]–[22] remains low in particular for large mission areas with randomly distributed sensor nodes, recent efforts on trajectory

optimization have focused on reactive trajectories [23]–[27] where the AUV path is corrected in real-time and refined to cope the sudden changes during the operation. In [23]–[26], assuming acoustic signaling for data transmission, trajectory planning of the data mule AUVs is formulated as a traveling salesman problem (TSP) to minimize the AUV travel time [23], [24], or to maximize the value of information (VoI) from the sensors [25], [26]. In [27], assuming VLC for data transmission, the trajectory finding problem of the AUV is solved using a greedy algorithm under VoI constraints. While the works in [23]–[27] simply assume that the AUV follows a straight path between each two sensor nodes, our previous work [28] further considers the effect of ocean currents and optimizes the trajectory between each two nodes.

The underlying assumption in above works [18]–[28] is that the AUV is battery powered. Battery-powered AUVs are required to return to the shore or the support vessel after a certain period in order to get recharged whether or not their mission is complete. Solar-powered AUVs have been further proposed for long term deployments to address the energy limitations of battery-powered counterparts [29]. They can harvest power from the sun light and use the harvested power to perform the mission or to store it for later use. In the current literature [29], [30], it is commonly assumed that the solar-powered AUV resurfaces in the daylight hours and recharges its batteries using the solar energy on the water surface while conducting its assigned mission during the night time hours. However, the recent progress of solar cell technology enables to efficiently harvest sunlight for submerged nodes [31]. This therefore makes possible the solar-powered AUVs to harvest energy during its mission.

In previous works where battery-powered AUVs are considered [18]–[28], the energy consumption is mainly related to the mission trajectory defined to cover a given area of interest. Energy harvesting (EH) aware trajectory optimization for solar-powered AUVs might indicate a conflicting trajectory to maximize the harvested energy, e.g., being closer to sea surface. In this paper, we formulate three-dimensional (3D) trajectory optimization for solar-powered AUVs with the goal of maximizing the harvested energy under constraints imposed by the data transmission. The optimization constraints include a fixed amount of data to be retrieved by the AUV from each node, therefore a corresponding transmission spectral efficiency and time duration. We formulate the problem as a bilevel optimization problem. The lower-level objective function is TSP which determines the optimum sequence order of the sensor nodes to be visited while the upper-level objective function is the optimization of the trajectory between each pair of adjacent nodes for the given order of node visits. Our numerical results demonstrate that the proposed trajectory significantly prolongs the mission time and autonomous operation of solar-powered AUV without the need to return to home base.

The rest of the paper is organized as follows: In Section II, we present the system model including energy harvesting, energy consumption, and optical communication models. In Section III, we formulate and solve the trajectory optimization problem. In Section IV, we provide numerical results and discussions on the performance in representative geographical locations. We finally conclude in Section V.

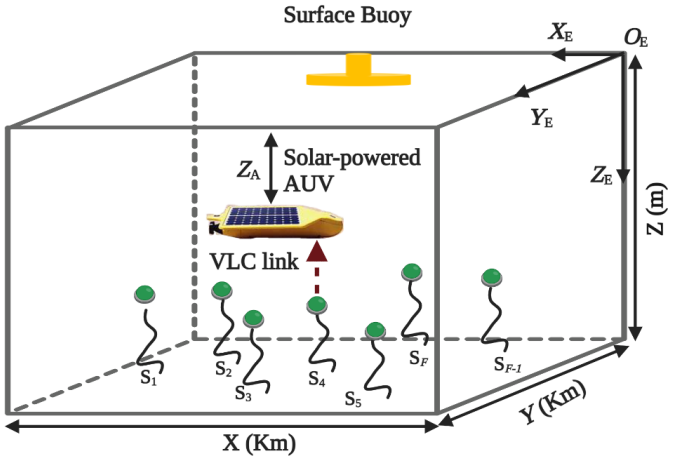

Fig. 1. Underwater sensor network under consideration.

II. System Model

As illustrated in Fig.1, we consider a three-dimensional USN scenario that covers a marine area of $X\ (\mathrm{km}) \times Y\ (\mathrm{km}) \times Z\ (\mathrm{km})$. It consists of a total of F randomly distributed sensor nodes, $\mathrm{S}_i\ i = 1, 2, ..., F$, with position vector $\mathbf{p}_{\mathrm{S}_i} = (x_{\mathrm{S}_i}, y_{\mathrm{S}_i}, z_{\mathrm{S}_i})$ anchored to the bottom of the sea with different heights. It is assumed that the three-dimensional underwater space map and the sensors' locations are readily available at the AUV[1].

A. Motion Model

We assume the deployment of a hybrid AUV [17] which has both propeller engine and buoyancy engine. It uses propeller engine to operate at relatively high speeds while it uses buoyancy engine to glide (i.e., float up and dive in) [16]. As illustrated in Fig. 2, the AUV is assumed to operate in four different modes, namely *communication*, *floating*, *thrust*, and *diving*, modes which are elaborated below:

- **Communication mode**: When the AUV visits a sensor node for data gathering, it switches to the communication mode during which it maintains a certain distance with the sensor node during the data transfer. In this mode, the buoyancy of the vehicle is made equal to the buoyancy of the water at the desired depth [16], known as "neutrally buoyant" position to keep the AUV (nearly) motionless.
- **Floating mode**: After the communication link is terminated, the AUV uses buoyancy engine to climb up. For this purpose, the vehicle's buoyancy is made less than that of the sea water so that the vehicle can float up to reach a desired depth [16].
- **Thrust mode**: In the thrust mode, the AUV uses its propeller engine to go forward. During this mode, it possesses a high maneuverability capability but at the cost of consuming more power for the operation [14].

[1]Commercially available solutions are available, see e.g., [32], [33] for underwater positioning and navigation.

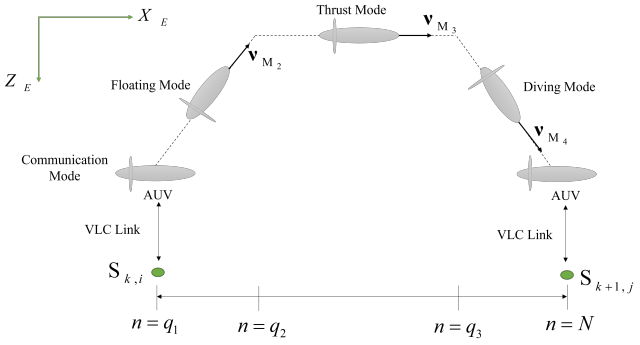

Fig. 2. Operation modes of AUV.

- **Diving mode**: To visit the next sensor node, the AUV stops the propeller engine and uses the buoyancy engine for diving. For this purpose, the vehicle's buoyancy is made greater than that of the sea water so that the vehicle can dive down to reach a desired depth [16].

Assume that the AUV starts from the node S_1, which is the closest node to its home base (i.e., support vessel, port, etc). Let $\mathbf{S} = (\mathrm{S}_{1,1}, \mathrm{S}_{2,i}, ..., \mathrm{S}_{k,i}, ..., \mathrm{S}_{F,i})$ $i \in \{2, ..., F\}$ denote the vector that describes the optimal sequence order of sensor node visits (see Section III for the related optimization). For example, $\mathrm{S}_{k,i}$ indicates that the sensor S_i was visited in the k^{th} order. Let $T = \sum_{k=1}^{F} T_k$ denote the mission time of AUV where T_k is the travel time from the sensor $\mathrm{S}_{k,i}$ to the sensor $\mathrm{S}_{k+1,j}$, $k = 1, 2, ..., F$, $j \neq i$, $j = 1, 2, ..., F$. This is divided into N equal-length time slots each with a duration of $\delta t_k[n] = T_k/N$. If δt_k is chosen sufficiently small, the location of the AUV can be assumed to be fixed during each time slot. The position of the AUV during its travel from $\mathrm{S}_{k,i}$ to $\mathrm{S}_{k+1,j}$ can be therefore described by the vector $\mathbf{p}_{\mathrm{A},k}[n] = (x_{\mathrm{A},k}[n], y_{\mathrm{A},k}[n], z_{\mathrm{A},k}[n])$, $n = 1, 2, .., q_1, .., q_2, .., q_3, .., N$ where q_1, q_2, q_3, and N denote switching times between different modes of operation (see Fig.2). Let $\nu_{\mathrm{M}}[n] = (v_{\mathrm{M},x}[n], v_{\mathrm{M},y}[n], v_{\mathrm{M},z}[n])$ denote the velocity of the AUV for a given operation mode $\mathrm{M} \in \{\mathrm{M}_1, \mathrm{M}_2, \mathrm{M}_3, \mathrm{M}_4\}$ where M_1, M_2, M_3, and M_4 respectively denote communication, floating, thrust, and diving modes. It can be noted that the vehicle remains nearly motionless in the communication mode, i.e., $\nu_{\mathrm{M}_1}[n] = (0, 0, 0)$ [2]. Therefore, we can formulate the AUV state as

$$\mathbf{p}_{\mathrm{A},k}[n] = \begin{cases} \mathbf{p}_{\mathrm{A},k}[n-1], n = 1, 2, ..., q_1 \\ \mathbf{p}_{\mathrm{A},k}[n-1] + (\nu_{\mathrm{o}}[n] + \nu_{\mathrm{M}_2}[n])\,\delta t_k[n], \quad n = q_1, ..., q_2 \\ \mathbf{p}_{\mathrm{A},k}[n-1] + (\nu_{\mathrm{o}}[n] + \nu_{\mathrm{M}_3}[n])\,\delta t_k[n], \quad n = q_2, ..., q_3 \\ \mathbf{p}_{\mathrm{A},k}[n-1] + (\nu_{\mathrm{o}}[n] + \nu_{\mathrm{M}_4}[n])\,\delta t_k[n], \quad n = q_3, ..., N \end{cases} \tag{1}$$

where $\nu_{\mathrm{o}}[n] = [\nu_{\mathrm{o},x}[n], \nu_{\mathrm{o},y}[n], \nu_{\mathrm{o},z}[n]]$ is the random vector quantifying the ocean current speed [17]. Specifically, $\nu_{\mathrm{o},x}[n]$ and $\nu_{\mathrm{o},y}[n]$ are modeled as independent Gaussian random variables with mean value of α and variance of β. Since the velocity of the ocean currents in the Z_{E} direction is negligible, $\nu_{\mathrm{o},z}[n]$ is assumed to be zero [35].

[2]The AUV may be subject to sways due to ocean currents and other disturbances in underwater environments which cannot be completely compensated by the buoyant engine. This may result in pointing errors as a result of misalignment between transmitter and receiver. Pointing-acquisition-tracking (PAT) methods can be used [13], [34] to handle such residual pointing errors.

B. Energy Consumption Model

The power consumption is calculated as the summation of power consumed for the movement of the vehicle and the power consumed by all other subsystems (i.e., communication, control, lighting, etc.) other than movement. The latter is called "hotel load" and is a negligible amount compared to the power consumption of the propeller engine [36]. Therefore, we assume the consumed power during communication mode is zero, i.e., $\Phi_{\mathrm{out}}[n] = 0$ for $n = 1, 2, ..., q_1$. In floating and diving modes, the power consumption for the vehicle's movement in the gliding process is the power used to pump the water in and out of the density control chamber to change the buoyancy and can be assumed negligible[3]. Therefore, we have $\Phi_{\mathrm{out}}[n] = 0$ for $n = q_1, ..., q_2$ and $n = q_3, ..., N$. In the thrust mode, assuming that the AUV moves with a constant speed [14], the consumed power is constant during each time slot and is given by

$$\Phi_{\mathrm{out}} = \frac{\rho}{2\eta_{\mathrm{p}}} C_{\mathrm{D}} A_{\mathrm{s}} \|\nu_{\mathrm{M}_3}\|^3, \tag{2}$$

where $\|.\|$ denotes the Euclidean vector norm, η_{p} is the efficiency of the propulsion system, ρ is the density of the water, and C_{D} is the drag resistance coefficient. In (2), A_{s} is the wetted surface area of the AUV and is given by [38]

$$A_{\mathrm{s}} = 2\pi \frac{{D_{\mathrm{s}}}^2}{4} \left(1 + \frac{L}{D_{\mathrm{s}}\sqrt{1 - {D_{\mathrm{s}}}^2/L^2}} \sin^{-1}\left(\sqrt{1 - {D_{\mathrm{s}}}^2/L^2}\right)\right) + A_{\mathrm{wings}}, \tag{3}$$

where $D_{\mathrm{s}} = \sqrt{6m/\rho\pi L}$, m is the mass, L is the length of the AUV, and A_{wings} is the surface area of its wings.

The energy consumption in each time slot is

$$E_{\mathrm{out},k}[n] = \Phi_{\mathrm{out}} \delta t_k[n] \cdot \tag{4}$$

The total energy consumption of the AUV to complete the mission (i.e., visiting F sensors in the mission area) is then calculated as $E_{\mathrm{out}} = \sum_{k=1}^{F} \sum_{n=q_2}^{q_3} E_{\mathrm{out},k}[n]$.

C. Energy Harvesting Model

As depicted in Fig.3.a, the overall solar intensity above the water includes direct and diffuse irradiances. A portion of direct and diffuse irradiances reflects from the air-water interface and a portion of it is refracted through the surface to the water [39]. The refracted portion will then pass through the water while facing attenuation in its way to reach the AUV. Thus, the received solar energy at a specific depth is affected by many factors including attenuation of the light intensity due to absorption and scattering, active surface area of the solar panel attached to the vehicle, and the solar panel's efficiency.

[3]In [37], assuming a velocity of $\nu_{\mathrm{M}_2} = \nu_{\mathrm{M}_4} = 0.4\,\mathrm{m/s}$ during floating and diving modes and a depth of $z_{\mathrm{A}} = 200\,\mathrm{m}$, the average energy consumption is reported to be less than 20 kJ. This is magnitudes of orders smaller than the energy consumption in the thrust mode (which is in the order of tens of MJ) and can be safely neglected in the analysis

Mathematically speaking, the harvested power by the AUV during the n^{th} time slot is given by [40]

$$\Phi_{\text{in},k}[n] = \xi\kappa\Psi_{0,\text{water}}[n]\exp\left(-cz_{\text{A},k}[n]\right).\cos\left(\Omega[n]\right), \quad (5)$$

where $z_{\text{A},k}[n]$ is the depth of the AUV, c is the extinction coefficient of the water, ξ is the solar panel efficiency, κ is the equivalent area of the solar panel, and Ω is the panel tilt. In (5), $\Psi_{0,\text{water}}$ is the light intensity right after passing through the water and given by

$$\Psi_{0,\text{water}}[n] = \left(1-\Upsilon_{\text{tot}}\right)\Psi_{0,\text{air}}[n], \quad (6)$$

where $\Psi_{0,\text{air}}[n]$ is the total intensity before entering the water (see Appendix I) and Υ_{tot} is the overall reflection of the solar direct irradiance from the ocean surface [40]. Assuming that the light is unpolarized and the water surface is flat, it can be calculated as the average of the reflectivity of the s-polarized and p-polarized light, i.e., $\Upsilon_{\text{tot}} = 0.5\left(\Upsilon_{\text{s}}[n] + \Upsilon_{\text{p}}[n]\right)$ where $\Upsilon_{\text{s}}[n]$, and $\Upsilon_{\text{p}}[n]$ are respectively given by

$$\Upsilon_{s}[n] = \left[\frac{n_1\cos\left(\varsigma[n]\right) - n_2 g[n]}{n_1\cos\left(\varsigma[n]\right) + n_2 g[n]}\right]^2. \quad (7)$$

$$\Upsilon_{p}[n] = \left[\frac{n_1 g[n] - n_2\cos\left(\varsigma[n]\right)}{n_1 g[n] + n_2\cos\left(\varsigma[n]\right)}\right]^2. \quad (8)$$

In the above, $g[n] = \sqrt{1-\left[\left(n_1/n_2\right)\sin\left(\varsigma[n]\right)\right]^2}$, and $\varsigma[n]$ is the solar zenith at time slot n (see Fig.3.b), n_1 and n_2 are the indexes of refraction for air and water respectively.

The harvested energy for a given time slot is

$$E_{\text{in},k}[n] = \Phi_{\text{in},k}[n]\,\delta t_k[n]\cdot \quad (9)$$

The total harvested energy by the AUV during its mission is then given by $E_{\text{in}} = \sum_{k=1}^{F}\sum_{n=1}^{N} E_{\text{in},k}[n]$.

D. Communication Model

Either LEDs or LDs can be used as transmitters in underwater VLC systems [11]. LEDs can provide relatively lower data rates as compared to LD-based systems. However, their divergence angle can relax the pointing-acquisition-tracking (PAT) requirements [13]. Based on the intended data rate and the level of PAT sub-system complexity that can be afforded, both light sources can be used. While the location information of sensor nodes are available at the AUV based on a three-dimensional underwater space map, it still needs to scan an uncertainty region centered about this initial position estimate [41] before the optical communication link can be established. After the sensor node is located, the AUV points its aperture towards the node and initiates the data transfer.

The spectral efficiency of VLC link (in bits/sec per unit bandwidth) is given by [42]

$$R_k[n] \geq \frac{1}{2}\log_2\left(1+\frac{e\left(rh_k[n]P\right)^2}{2\pi\sigma^2}\right), \quad (10)$$

where r is the detector responsivity, P is the transmit power, and σ^2 is the noise variance. In (10), $h_k[n]$ is the path loss between the AUV and the sensor node $\text{S}_{k,i}$ and is given by [43]

$$h_k[n] = \exp\left(-cd_{\text{A},k}[n]\right), \quad (11)$$

where $d_{\text{A},k}[n] = \left\|\mathbf{p}_{\text{A},k}[n] - \mathbf{p}_{\text{S}_{k,i}}\right\|$ is the link distance between the AUV and the sensor node $\text{S}_{k,i}$. The communication mode spans a total of $t_{\text{M}_1,k} = \sum_{n=1}^{q_1}\delta t_k[n]$ seconds during which the AUV stops and extracts data from the node. Given the link bandwidth of B, the retrieved data (in terms of bits) for this duration is

$$\Im_k = BR_k t_{\text{M}_1,k}. \quad (12)$$

Let $\Im_{\text{sc}}$ denote the storage capacity of each sensor node. The link parameters ($t_{\text{M}_1,k}$ and R_k) need to be selected to support this data retrieval, i.e., $\Im_k = \Im_{\text{sc}}$.

III. Optimal Trajectory

As described in the previous section, the AUV visits F sensor nodes and returns to the initial point after completing the mission. It takes N time slots to visit from one sensor node to the other. Therefore, the AUV's trajectory is defined by (13), as shown at the bottom of this page.

Let Q_{b} denote the initial battery energy (i.e., energy level at the start of the mission). The overall available energy in each time slot is $E_{\text{c},k}[n] = Q_{\text{b}} + E_{\text{in},k}[n]$. We define the net energy at each time slot as

$$E_{\text{net},k}[n] = E_{\text{c},k}[n] - E_{\text{out},k}[n]\cdot \quad (14)$$

In our work, we aim to maximize the net energy defined as $E_{\text{net}} = \sum_{k=1}^{F}\sum_{n=1}^{N} E_{\text{net},k}[n]$. It is obvious that E_{net} is directly affected by the visit sequence of sensor nodes and the path followed between two consecutive nodes. We formulate the problem as a bilevel optimization problem. The lower-level objective function is the minimization of the mission length d_{tot}. It is defined as

$$d_{\text{tot}} = \sum_{i=1}^{F}\sum_{j\neq i,j=1}^{F} d_{ij}b_{ij}, \quad (15)$$

where $d_{ij} = \left\|\mathbf{p}_{\text{S}_i} - \mathbf{p}_{\text{S}_j}\right\|$ is the distance between sensor nodes S_i and S_j $j\neq i$, $j = 1,2,...,F$. b_{ij} is set as 1 when there is a path between sensor S_i to sensor S_j, otherwise set as $b_{ij} = 0$. The upper-level objective function is maximization

$$\mathbf{P}_{\text{A}} = \left\{\underbrace{\mathbf{p}_{\text{A},1}[1]...\mathbf{p}_{\text{A},1}[N]}_{\text{Firstnode}}...\underbrace{\mathbf{p}_{\text{A},k}[1]...\mathbf{p}_{\text{A},k}[N]}_{k^{th}\text{node}}.....\underbrace{\mathbf{p}_{\text{A},F}[1]...\mathbf{p}_{\text{A},F}[N]}_{F^{th}\text{node}}\ \underbrace{\mathbf{p}_{\text{A},1}[1]...\mathbf{p}_{\text{A},1}[N]}_{\text{Firstnode}}\right\}. \quad (13)$$

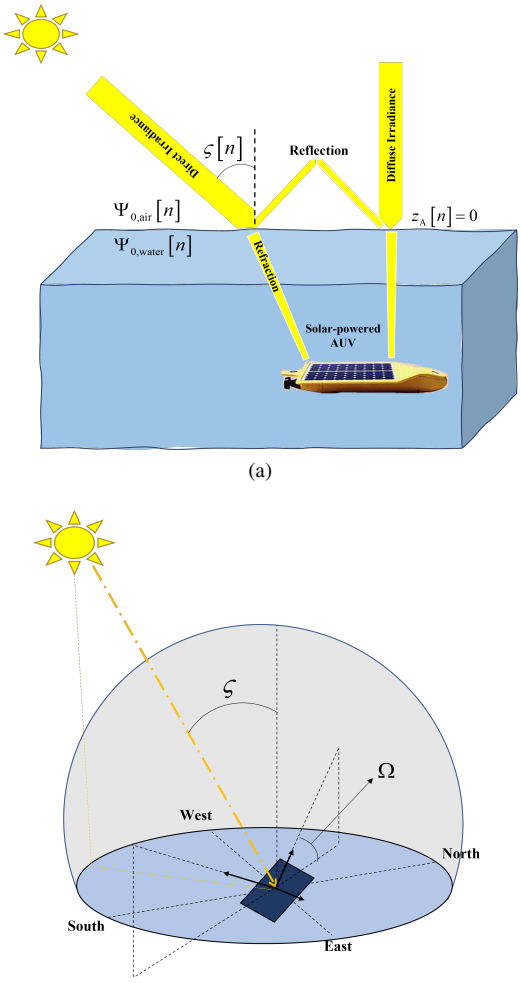

Fig. 3. (a) Solar irradiance and various effects on them in their way of reaching the destination, (b) Geometry of solar panel with respect to sun.

of the net energy, E_{net}, during the mission for the optimized sequence order of node visits obtained from the lower-level optimization. Mathematically speaking, we have

$$\begin{aligned} &\max_{\mathbf{p}_{\text{A}}} \; E_{\text{net}} \\ &\text{s.t.} \quad \text{C1}: \Im_k = \Im_{\text{sc}}, \qquad \forall\, k = 1, ..., F \\ &\qquad \text{C2}: \Phi_{\text{in},k}[n] \geq \Phi_{\text{th}}, \;\; \forall\, n = q_2, ..., q_3 \end{aligned} \quad , \tag{16}$$

where the optimal visit sequence of sensor nodes is obtained from

$$\begin{aligned} &\min_{\mathbf{b}} \; d_{\text{tot}} \\ &\text{s.t.} \quad \text{C3}: \sum_{j=1, j\neq i}^{F} \sum_{i=1}^{F} b_{ij} = 1\,, \;\; \sum_{i=1, i\neq j}^{F} \sum_{j=1}^{F} b_{ij} = 1 \\ &\qquad \text{C4}: \sum_{i\in\Xi} \sum_{j\neq i, j\in\Xi} b_{ij} \leq |\Xi| - 1, \;\; \forall \Xi \subseteq \{1, 2, ..., F\} \end{aligned} \quad . \tag{17}$$

The constraint C1 imposes that the full amount of data stored on each sensor node is completely retrieved during the period of communication mode. The transmission time duration ($t_{\text{M}_1,k}$) and transmission spectral efficiency (R_{th}) should be selected to support this data retrieval. For a fixed value for R_{th}, the required time duration for data transfer can be obtained using (12). To achieve the selected value of R_{th}, the AUV needs to maintain a certain distance of d_{th} from the sensor nodes, i.e., $\left\|\mathbf{p}_{\text{A},k} - \mathbf{p}_{\text{S}_{k,i}}\right\| = d_{\text{th}}$ during these $t_{\text{M}_1,k}$ seconds. Based on (10) and (11), we can write

$$d_{\text{th}} \leq \frac{1}{2c} \ln \left[\left(\frac{2\pi\sigma^2}{er^2 P} \left(2^{2R_{\text{th}}} - 1\right) \right)^{-1} \right]. \tag{18}$$

Accordingly, the operation depth of the AUV during the communication mode must satisfy $z_{\text{A,k}} \geq \Delta_{\min,k}$ where $\Delta_{\min,k}$ is given by

$$\Delta_{\min,k} = z_{\text{S}_{k,i}} - d_{\text{th}}. \tag{19}$$

The constraint C2 imposes a minimum required power (denoted by Φ_{th}), which dictates a maximum operation depth $\Delta_{\max}$ for the AUV in the thrust mode, i.e., $q_2 \leq n \leq q_3$, which is obtained from (5) as

$$\Delta_{\max} = \frac{1}{c} \ln \left(\frac{\Phi_{\text{th}}}{\xi\kappa\Psi_{0,\text{water}} \cos(\Omega)} \right)^{-1}. \tag{20}$$

Constraint C3 implies that each sensor is visited exactly once. In constraint C4, Ξ is any sequence of sensor nodes that can form a sub-tour instead of one single tour. It enforces that there is only a single tour covering all sensor nodes, and not multiple disjointed tours.

The lower level objective function is in the form of a traveling salesman problem (TSP), which is an NP-hard problem [44]. It can be solved using nearest neighbor (or greedy) algorithms [21], [27] or evolutionary algorithms such as the genetic algorithm [45], particle swarm optimization [46], and ant colony algorithm [7]. Here, we use genetic algorithm due to the fact that the crossover feature of genetic algorithm makes it more powerful than other evolutionary algorithms in solving TSP [47]. The genetic algorithm relies on a population of individuals that simultaneously explores the search space and generates new solutions by recombining individuals of the current population. The output of lower-level optimization is a matrix with zero and one entries from which we extract the sequence order of sensor nodes to be visited and therefore construct the vector (see Appendix II).

Having the optimum sequence order of the sensor nodes, we solve the upper-level objective function of (16) numerically using fmincon function [48] of the MATLAB optimization toolbox. This function is based on the trust-region algorithm and is defined to carry out the optimization by using the present information and then repeat the process over and over until it reaches a convergence. Accordingly, with knowledge of the start and the end points of the movement and the underwater current speed in each time slot, the best trajectory between the two sensor nodes is determined.

The flowchart of the proposed algorithm for trajectory planning is provided in Table I. The inputs of the upper-level optimization problem include the number of sensor nodes (F), the number of time slots (N), the minimum required depth ($\Delta_{\min,k}$) to satisfy the data rate constraint, the maximum depth ($\Delta_{\max}$) to satisfy the minimum levels of harvested power, the storage capacity of sensor nodes ($\Im_{\text{sc}}$), the velocity of the AUV ($\|\nu_{\text{M}}\|$) in addition to the optimum sequence order of sensors to be visited. The optimum sequence order of sensor nodes

TABLE I
FLOWCHART FOR THE PROPOSED EH-AWARE TRAJECTORY PLANNING ALGORITHM

Initialization:
Set F, N, $\Delta_{\min,k}$, $\Delta_{\max}$, $\|\nu_{\mathrm{M}}\|$, $\Im_{\mathrm{sc}}$
$\mathbf{S} \leftarrow \left(\mathrm{S}_{1,1}, \mathrm{S}_{2,i}, ..., \mathrm{S}_{k,i}, ..., \mathrm{S}_{F,i}\right)$, $i \in \{2, ..., F\}$
Update and finding the optimal solution:
for $k = 1$ to F
if $z_{\mathrm{A},k}[n] \geq \Delta_{\min,k}$
$\mathrm{M} \leftarrow \mathrm{M}_1$ (switch to communication mode), $n \leftarrow 1$
end if
if $\Im_k = \Im_{\mathrm{sc}}$ (number of received bits)
$\mathrm{M} \leftarrow \mathrm{M}_2$ (switch to floating mode), $n \leftarrow q_1$
end if
if $z_{\mathrm{A},k}[n] \leq \Delta_{\max}$
$\mathrm{M} \leftarrow \mathrm{M}_3$ (switch to thrust mode), $n \leftarrow q_2$
end if
for $n = q_2$ to $n = q_3$
Update and interpolate the ocean current vector fields $\nu_{\mathrm{o}}[n]$
$\delta t_k[n] \leftarrow \frac{\|\mathbf{p}_{\mathrm{A},k}[n] - \mathbf{p}_{\mathrm{A},k}[n-1]\|}{\|\nu_{\mathrm{o}}[n] + \nu_{\mathrm{M}}[n]\|}$
Update the upper-level optimization problem of (16)
Maximize E_{net}
$\mathbf{p}_{\mathrm{A},k}[n] \leftarrow \left(x_{\mathrm{A},k}[n], y_{\mathrm{A},k}[n], z_{\mathrm{A},k}[n]\right)$
end for
if $z_{\mathrm{A},k+1} \leq \Delta_{\min,k+1}$
$\mathrm{M} \leftarrow \mathrm{M}_4$ (switch to diving mode), $n \leftarrow q_3$
else if
$\mathrm{M} \leftarrow \mathrm{M}_1$, $n \leftarrow N$
end if
end for
Output: $\mathbf{P}_{\mathrm{A}}$

(denoted by $\mathbf{S}$) is the output of the lower-level optimization problem and is stored on the AUV before the mission start. During the mission, the AUV executes the solution of upper-level optimization problem in real time which deals with the optimization of the path between each two adjacent sensors. The AUV starts from sensor $\mathrm{S}_{1,1}$ which is the closest node to the base station. Driven by buoyancy engine, the AUV adaptively adjusts its depth until it satisfies the threshold data rate ($z_{\mathrm{A},k} \geq \Delta_{\min,k}$). It then switches to the communication mode ($\mathrm{M} \leftarrow \mathrm{M}_1$). The AUV sends a wake-up signal for the sensor to establish the link and start transferring the data. After it retrieves $\Im_k = \Im_{\mathrm{sc}}$ bits, the node goes to sleep and the AUV switches to floating mode ($\mathrm{M} \leftarrow \mathrm{M}_2$) at $n = q_1$. Using buoyancy engine, it floats up until it reaches a suitable depth near the water surface ($z_{\mathrm{A},k} \leq \Delta_{\max}$). At time slot $n = q_2$, it switches to thrust mode ($\mathrm{M} \leftarrow \mathrm{M}_3$) during which the AUV is driven by the propeller engine until time slot $n = q_3$. It then switches to diving mode ($\mathrm{M} \leftarrow \mathrm{M}_4$) and gets close to the next sensor node using buoyancy engine. During this mode, it adjusts its depth taking into account the required transmission distance for data transfer. At time slot $n = N$ (when its distance to the next sensor node is close enough to satisfy the threshold data rate), it switches to communication mode again, and the same process will be repeated until it visits all the sensor nodes.

IV. NUMERICAL RESULTS

In this section, we first present the potential levels of underwater harvested energy for a given operation depth, water type, and geographical location. Then we present our numerical results for the trajectory optimization and discuss the improvement in net energy made possible through this optimization. Unless otherwise stated, system and channel parameters are provided in Table II while AUV specifications are further provided in Table III. The populations and the number of iterations in the genetic algorithm are set as 100 and 10000, respectively. The storage capacity of each sensor node is $\Im_{\mathrm{sc}} = 256\,\mathrm{Mbits}$ [49]. Therefore, the total data to be collected from $F = 18$ sensor nodes is equal to $\Im_{\mathrm{sc}} = 4.608\,\mathrm{Gbits}$.

The amount of harvested energy is obviously dependent on the time of the day and geographical location. We assume four representative days of the year, namely January 1^{st} (i.e., $\Theta = 1$), March 30^{th} ($\Theta = 90$), June 28^{th} ($\Theta = 180$), and September 26^{th} ($\Theta = 270$). In addition, we consider three climate types including tropical (also known as equatorial, which is close to the equator), mid-latitude (between the latitudes of $\vartheta = 23°$ and $\vartheta = 66°$ in the north and between the latitudes of $\vartheta = -23°$ and $\vartheta = -66°$ in the south polar region of earth), and subarctic (region in the northern hemisphere near the arctic ocean). As examples, we consider

- Indian Ocean with latitude of $\vartheta = 0.06°$ and longitude of $\theta = 63.72°$ (representative of tropical climate type),
- Arctic Ocean with latitude of $\vartheta = 65.24°$ and longitude of $\theta = -60.46°$ (representative of subarctic climate type), and
- Black Sea with latitude of $\vartheta = 41.8°$ and longitude of $\theta = 37.6°$ (representative of mid-latitude climate type).

The panel tilt is assumed to be zero, i.e., $\Omega[n] = 0\ \forall n$, and the solar powered AUV is assumed to be located on the sea surface, i.e., $z_{\mathrm{A}} = 0$. Fig.4 illustrates the hourly variations of the harvested power using (5) in tropical, subarctic, and mid-latitude climate types under consideration for different seasons. Comparison of these figures reveals that there might be significant differences in the amount of harvested energy depending on the time of the day, specific season and geographical location. For geographical locations and the representative days under consideration, the maximum harvested power is obtained around $w_{\max} = 12$ (when the zenith angle is at a minimum level) except in the mid-latitude climate type and on $\Theta = 180^{\mathrm{th}}$ day of the year where it is obtained at $w_{\max} = 11$. The determination of $w_{\max}$ is critical to achieve the best performance in terms of energy harvesting while planning the mission. If the AUV's mission time takes T hours, the AUV should start its mission $T/2$ hours before $w_{\max}$ so it can hit $w_{\max}$ just in the middle of the mission. The best start time is then determined as $t_{\mathrm{start}} = |w_{\max} - T/2|$.

It should also be noted that the daylight hours are different for these locations. For example, in subarctic climate type, the maximum and minimum daylight duration is 19 and 5 hours, respectively, in $\Theta = 180^{\mathrm{th}}$ and $\Theta = 1^{\mathrm{st}}$ day of the year. In tropical climate, the daylight duration is the same (14 hours) for all the representative days. Morover, there is not much difference between the amount of harvested power in different days of the year for this location, while for subarctic and mid-latitude locations, the specific season has a significant effect. For example, maximum and minimum levels of harvested power are obtained as $\Phi_{\mathrm{in,max}} = 222.1\,\mathrm{W}$ and $\Phi_{\mathrm{in,min}} =$

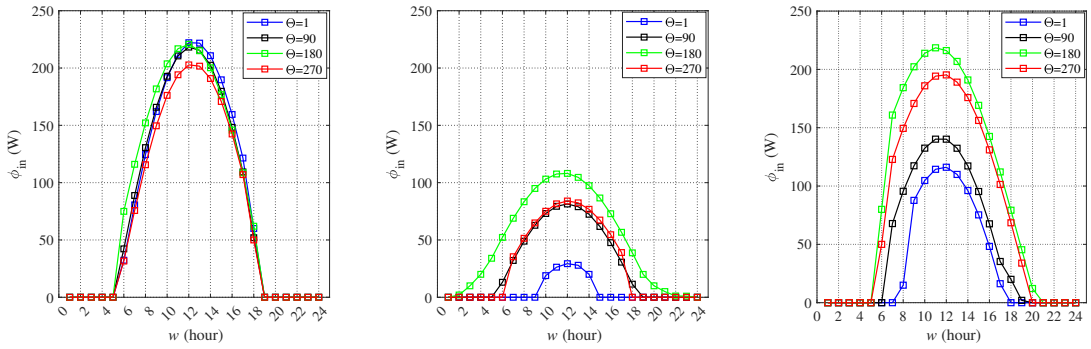

(a) (b) (c)

Fig. 4. Hourly variation of harvested power on the sea surface for different days in climate type of (a) Tropical, (b) Subarctic, (c) Mid-latitude.

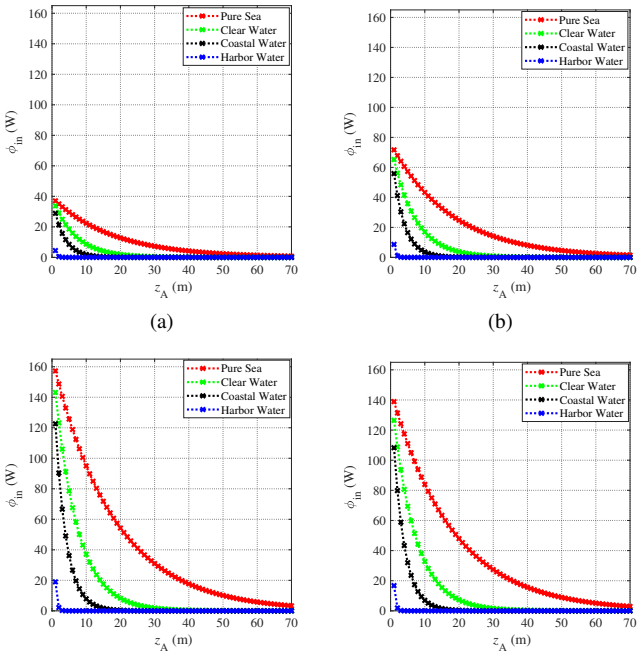

(a) (b) (c) (d)

Fig. 5. Average amount of harvested power with respect to depth for different water types on (a) 1^{st} day, (b) 90^{th} day, (c) 180^{th} day, (d) 270^{th} day of the year.

202.7 W respectively for $\Theta = 1^{\text{st}}$ and $\Theta = 270^{\text{th}}$ day of the year for tropical climate type. These significantly decrease for the representative subarctic location where maximum and minimum levels are observed as $\Phi_{\text{in,max}} = 108.1\,\text{W}$ and $\Phi_{\text{in,min}} = 29.31\,\text{W}$ respectively for $\Theta = 180^{\text{th}}$ and $\Theta = 1^{\text{st}}$ day of the year.

In the following, we assume the mid-latitude climate type (Black Sea location) as an example. Fig.5 illustrates the average amount of harvested power (averaged over daytime hours) with respect to operation depth for different water types. For example, on the $\Theta = 180^{\text{th}}$ day of the year, when the AUV is close to the sea surface (i.e., $z_{\text{A}} \leq 1\,\text{m}$), it is capable of harvesting an average amount of $\Phi_{\text{in}} \geq 161\text{W}$, $\Phi_{\text{in}} \geq 146.5\text{W}$, $\Phi_{\text{in}} \geq 125.5\text{W}$, and $\Phi_{\text{in}} \geq 19.4\text{W}$ in pure sea, clear water, coastal water, and harbor water, respectively.

TABLE II
SYSTEM AND CHANNEL PARAMETERS

Parameter	Variable	Value
Mission area	$X{\times}Y{\times}Z$	$20{\times}20{\times}0.03$ km^3
Number of sensor nodes	F	18
Number of time slots	N	1000
Mean of ocean current speed	α	$0.6\,\text{m/s}$
Variance of ocean current speed	β	0.01
Transmit power	P_{t}	0.01W
Detector responsivity	r	0.5
Noise variance	σ^2	10^{-11}W
Bandwidth of the channel	B	100 MHz
Storage capacity of sensor nodes	$\Im_{\text{sc}}$	256 Mbits
Minimum required spectral efficiency	R_{th}	8 bits/sec/Hz
Minimum level of harvested power	Φ_{th}	80 W
Refractive index of air	n_1	1
Refractive index of water	n_2	1.33
Extinction coefficient for pure sea	c	0.056 m^{-1}
Extinction coefficient for clear ocean	c	0.015 m^{-1}
Extinction coefficient for coastal water	c	0.305 m^{-1}
Extinction coefficient for harbor water	c	2.17 m^{-1}
Latitude of the location of interest	ϑ	41.8°
Longitude of the location of interest	θ	37.6°
Day of the year	Θ	180
Solar constant	Ψ	1366 W/m^2

As the depth increases, the harvested energy diminishes. For example, in pure sea, when the depth is less than 70 m, the harvested energy becomes negligible. As turbidity increases, the required depth further decreases. The harvested energy becomes zero for $z_{\text{A}} \geq 70\,\text{m}$, $z_{\text{A}} \geq 35\,\text{m}$, $z_{\text{A}} \geq 15\,\text{m}$, and $z_{\text{A}} \geq 2\,\text{m}$, respectively, for clear water, coastal water, and harbor water. These results indicate that the AUV is indeed capable of harvesting power even when operating underwater. However, the amount of harvested energy is significantly dependent on the water type as well as the operation depth. This shows the importance of EH-aware three-dimensional (3D) trajectory optimization taking into account the operation depth.

To demonstrate the benefits of trajectory optimization, we consider a coastal marine area with a size of $X \times Y \times Z = 20\,\text{Km} \times 20\,\text{Km} \times 30\,\text{m}$ as an example with $F = 18$ sensors with location vectors provided in Table IV. We assume that the mission is done in Black Sea with latitude of $\vartheta = 41.8°$ and longitude of $\theta = 37.6°$,

TABLE III
SPECIFICATIONS OF THE SOLAR-POWERED AUV

Parameter	Variable	Value
Length of the solar-powered AUV	L	1.8 m [50]
Mass of the solar-powered AUV	m	75.5 Kg [50]
Diameter of the solar-powered AUV	$D_{\rm s}$	0.14 m [50]
Surface area of the solar panel	κ	1m × 1m [51]
Wing area	$A_{\rm wings}$	$0.127\,{\rm m}^2$ [17]
Drag coefficient	$C_{\rm D}$	0.0064 [50]
Efficiency of the propulsion system	$\eta_{\rm p}$	73% [50]
Efficiency of the solar panel	ξ	20% [51]
Velocity of the AUV (thrust mode)	$\|\nu_{\rm M_3}\|$	2 m/s [17]
Velocity of the AUV (floating mode)	$\|\nu_{\rm M_2}\|$	0.4 m/s [17]
Velocity of the AUV (diving mode)	$\|\nu_{\rm M_4}\|$	0.4 m/s [17]
Initial battery storage size	$Q_{\rm b}$	36 MJ [50]
Water density	ρ	$997\,{\rm Kg/m}^3$ [17]

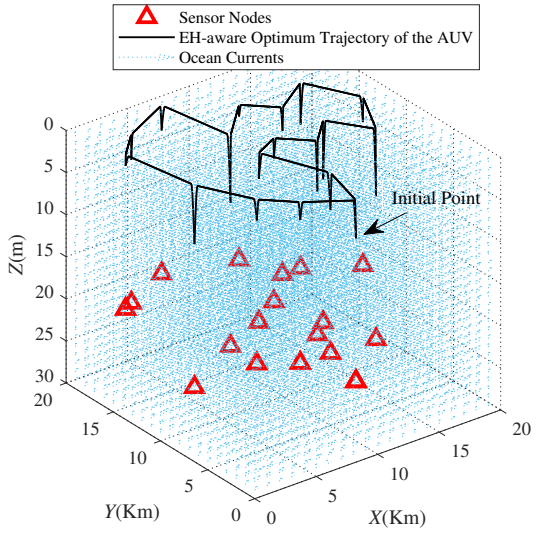

(a)

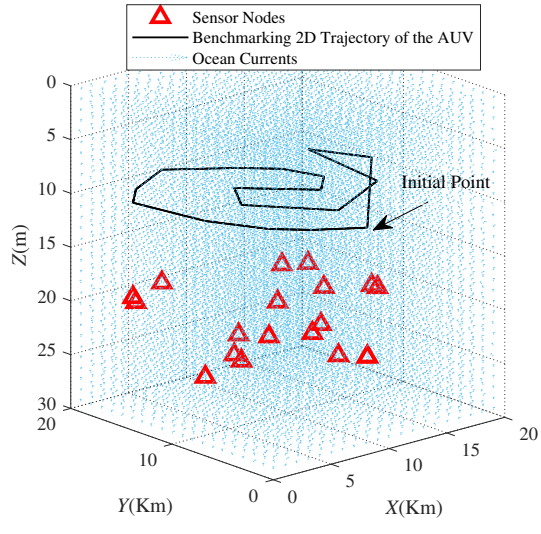

(b)

Fig. 6. (a) Optimal 3D EH-aware trajectory, (b) Benchmarking 2D trajectory.

the date is June 28th ($\Theta = 180^{\rm th}$), the water is coastal type, and $w_{\max} = 11\,{\rm am}$. As discussed in the previous section, we first solve (17) using genetic algorithm and obtain the optimum sequence order of sensor nodes as $\mathbf{S} = (\mathrm{S}_{1,1}, \mathrm{S}_{2,4}, \mathrm{S}_{3,2}, \mathrm{S}_{4,6}, \mathrm{S}_{5,5}, \mathrm{S}_{6,3}, \mathrm{S}_{7,17}, \mathrm{S}_{8,9}, \mathrm{S}_{9,10}, \mathrm{S}_{10,18}, \mathrm{S}_{11,8}, \mathrm{S}_{12,7}, \mathrm{S}_{13,12}, \mathrm{S}_{14,16}, \mathrm{S}_{15,11}, \mathrm{S}_{16,14}, \mathrm{S}_{17,13}, \mathrm{S}_{18,15})$. For the given order, we then solve (16) to yield the optimal trajectory illustrated in Fig. 6.a. The optimal operation depth at each sensor node is the minimum required depth for the AUV to satisfy the constraint C1 and is obtained in accordance with each sensor's height using (19).

TABLE IV
SENSOR LOCATIONS

Sensor S_i	$\mathbf{p}_{\mathrm{S}_i}$ (Km, Km, m)	Sensor S_i	$\mathbf{p}_{\mathrm{S}_i}$ (Km, Km, m)
S_1	$(9, 1, 25)$	S_{10}	$(11, 16, 23)$
S_2	$(4, 5, 19.5)$	S_{11}	$(12, 9, 19)$
S_3	$(3, 17, 21)$	S_{12}	$(16, 8, 19.4)$
S_4	$(6, 3, 22)$	S_{13}	$(6, 10, 20)$
S_5	$(1, 15, 19.3)$	S_{14}	$(10, 11, 20)$
S_6	$(2, 9, 20)$	S_{15}	$(10, 5, 24)$
S_7	$(19, 12, 25)$	S_{16}	$(14, 11, 19.8)$
S_8	$(17, 16, 20.1)$	S_{17}	$(7, 19, 22)$
S_9	$(8, 13, 27)$	S_{18}	$(13, 14, 19.4)$

As a benchmark (see Fig.6.b), we consider a two-dimensional (2D) trajectory where the AUV works at a fixed operation depth and follows a straight path between sensor nodes. In this case, the sequence order of sensor nodes is determined by the nearest neighbor algorithm and is given by $\mathbf{S} = (\mathrm{S}_{1,1}, \mathrm{S}_{2,4}, \mathrm{S}_{3,2}, \mathrm{S}_{4,6}, \mathrm{S}_{5,5}, \mathrm{S}_{6,3}, \mathrm{S}_{7,17}, \mathrm{S}_{8,10}, \mathrm{S}_{9,18}, \mathrm{S}_{10,16}, \mathrm{S}_{11,11}, \mathrm{S}_{12,14}, \mathrm{S}_{13,9}, \mathrm{S}_{14,13}, \mathrm{S}_{15,15}, \mathrm{S}_{16,12}, \mathrm{S}_{17,8}, \mathrm{S}_{18,7})$. The selection of fixed operation depth is made such that it guarantees a reliable transmission between the AUV and each of the nodes. For this example, the fixed operation depth is found as $z_{\rm A} = 9.5\,{\rm m}$[4]. For the given bandwidth of $B = 100\,{\rm MHz}$ and required spectral efficiency of $R_{\rm th} = 8\,{\rm bits/sec/Hz}$, it can be calculated from (12) that the required data of $\Im_{\rm sc} = 256\,{\rm Mbits}$ can be gathered in $t_{{\rm M}_1,k} = 0.32$ seconds. Moreover, to satisfy $R_{\rm th} = 8\,{\rm bits/sec/Hz}$, the distance between the AUV and the sensor node needs to be equal to $d_{\rm th}$ based on (18). In the 2D benchmarking case, since the operation depth is fixed, the distance between the AUV and each node to satisfy $R_{\rm th} = 8\,{\rm bits/sec/Hz}$ is less than $d_{\rm th}$ in most cases. The communication duration takes values in the range of $t_{{\rm M}_1,k} = 0.19 - 0.3$ seconds. The difference between two cases is obviously negligible given the mission time in terms of hours.

In Fig.7.a, we illustrate the consumed and harvested energy levels as well as the net energy over the mission duration for the EH-aware 3D optimum trajectory. We assume that the initial battery energy is $Q_{\rm b} = 36{\rm MJ}$ [50], so the net energy level at the start of the mission is $E_{\rm net} = 36\,{\rm MJ}$. Under the assumptions of $\|\nu_{\rm M_3}\| = 2{\rm m/s}$, $\|\nu_{\rm M_2}\| = \|\nu_{\rm M_4}\| = 0.4\,{\rm m/s}$, and $\|\nu_{\rm M_1}\| = 0\,{\rm m/s}$, the required mission time is $T = 9.59$ hours,

[4]In the USN scenario under consideration, the depth that guarantees the reliable transmission between the AUV and all the nodes (to satisfy the spectral efficiency of $R_k\,[n] \geq R_{\rm th}$) is $z_{\rm A} \geq 9.4\,{\rm m}$ which is dictated by the node with the highest depth amongst all. Therefore, in the benchmarking case with a fixed depth trajectory, we assume that the AUV swims at the depth of $z_{\rm A} = 9.5\,{\rm m}$.

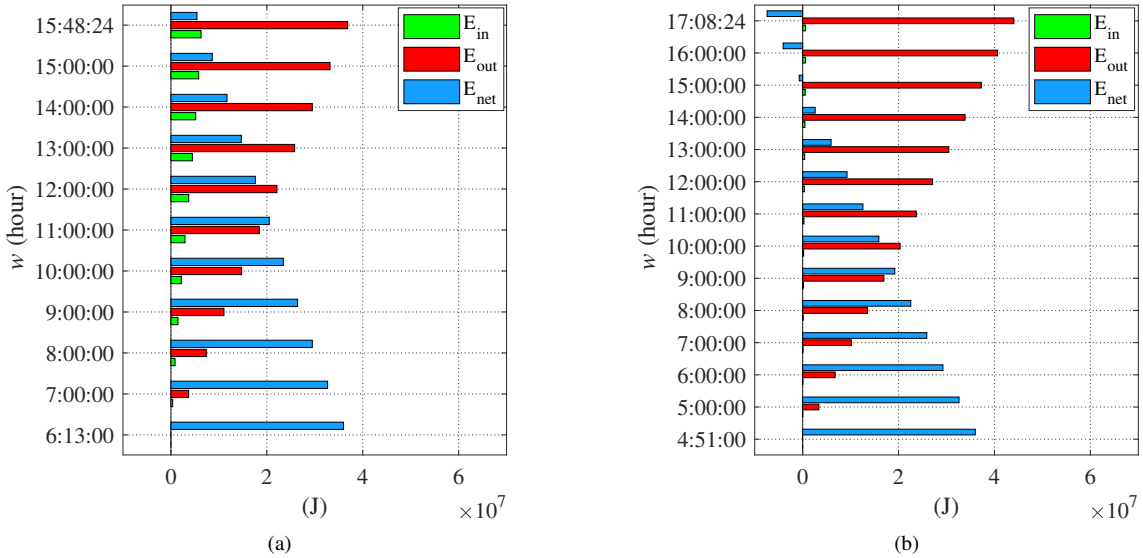

Fig. 7. Consumed, harvested and net energy levels over the mission duration (a) optimal 3D trajectory, (b) benchmark 2D trajectory.

and the corresponding mission length is $d_{\text{tot}} = 73.44\,\text{Km}$. Assuming that the mission is initiated at the best start time of $t_{\text{start}} = 6:13:00$, the total harvested energy during the mission is $E_{\text{in}} = 6.28\,\text{MJ}$ while the total consumed energy is $E_{\text{out}} = 36.8\,\text{MJ}$. Therefore, at the end of the mission, the remaining net energy is $E_{net} = Q_b + E_{in} - E_{out} = 5.43\text{MJ}$. This indicates that the AUV does not run out of battery and, by the time the mission is completed, it has an additional amount of 5.43MJ remaining in its battery.

In Fig.7.b, we illustrate the consumed, harvested and net energy levels for the benchmarking 2D trajectory. In this case, it takes $T = 12.29$ hours to complete the mission, and the corresponding mission length is $d_{\text{tot}} = 89.28\,\text{Km}$. The total consumed energy is $E_{\text{out}} = 44\text{MJ}$. Assuming that the mission starts at $t_{\text{start}} = 4:51:00$ (i.e., the best start time for this case), the total harvested energy is $E_{\text{in}} = 0.6\,\text{MJ}$. It can be readily seen that the AUV runs out of battery before $w = 15:00:00$. The net energy at the end of the mission is $E_{\text{net}} = -7.42\,\text{MJ}$, which indicates that the AUV would need this additional amount to complete the mission.

Fig.8 illustrates the effect of thrust mode's velocity on the AUV performance. It is observed that energy consumption increases proportional to the cube of velocity based on (2). It has also an indirect effect on the energy harvesting. According to (9), with the increase in the velocity, the time taken to go from one sensor to the next decreases and therefore less power can be harvested from the sun. Therefore, the net energy effectively decreases. For instance, assume a velocity of $\|\nu_{\text{M}_3}[n]\| = 3\,\text{m/s}$. The required mission time is $T = 6.4$ hours. The total harvested energy during the mission is $E_{\text{in}} = 4.2\,\text{MJ}$ while the total consumed energy is $E_{\text{out}} = 91.7\,\text{MJ}$. Therefore, at the end of the mission, there is an energy shortage in the amount of $E_{net} = Q_b + E_{in} - E_{out} = -51.46\text{MJ}$. On the other hand, if we decrease the velocity to $\|\nu_{\text{M}_3}[n]\| = 1\,\text{m/s}$, the required mission time is $T = 19.4$ hours. The total harvested energy during the mission is $E_{\text{in}} = 12.74\,\text{MJ}$ while

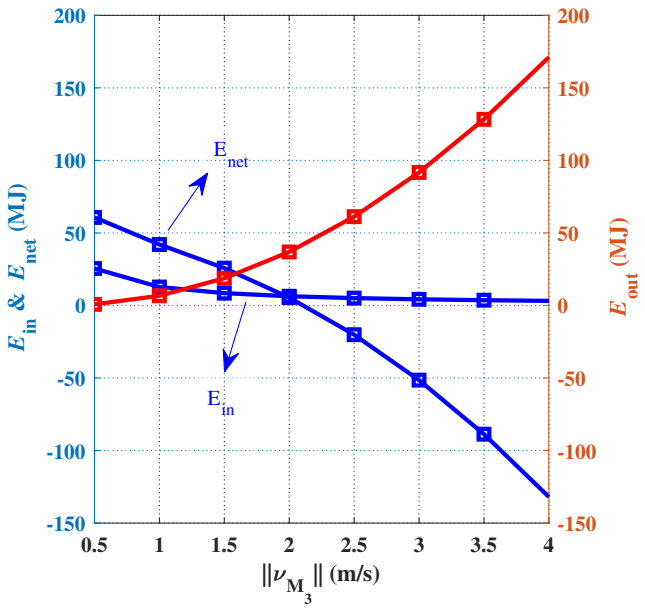

Fig. 8. Effect of velocity on the harvested energy, consumed energy, and net energy.

the total consumed energy is $E_{\text{out}} = 6.7\,\text{MJ}$. Therefore, at the end of the mission, the remaining net energy is $E_{net} = Q_b + E_{in} - E_{out} = 42\text{MJ}$. However, the operation time ($T = 19.4$ hours) significantly increases from 6.4 hours to 19.4 hours. This indicates the importance of properly selecting the velocity value to find the best trade-off between the net energy and operation time.

In Fig. 9, we compare the net energy levels for three climate types under consideration and the representative operation days. We consider the parameters provided in Table II and Table III. In the case of benchmarking 2D scheme, the

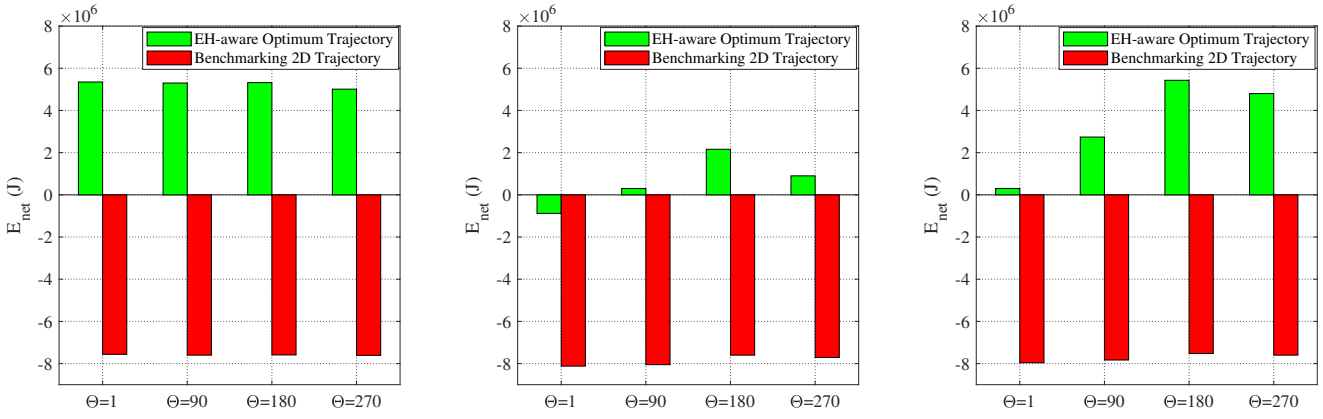

(a) (b) (c)

Fig. 9. Comparison of net energy levels for different operation days under consideration in (a) Tropical, (b) Subarctic, and (c) Mid-latitude climate types.

harvested energy remains very low values in all the climate types and, regardless of the operation day, this trajectory yields negative values for net energy indicating that the battery runs out before the mission time for the given size of area and the number of sensor nodes to be visited. In general, optimized trajectory yields much better performance in comparison to the 2D benchmarking scheme. The net energy level changes with the operation day since it is highly dependent on harvested energy level. For all operation days under consideration except the $\Theta = 1^{\text{st}}$ day of the year for the subarctic location, net energy levels always take positive values indicating that mission is successfully completed as a result of the adopted optimal EH-aware trajectory.

V. Conclusion

In this paper, we considered a USN network where the solar-powered AUV visits sensor nodes for data retrieval through a VLC link. We presented the potential levels of underwater harvested energy for different operation depths, water types on representative days and geographical locations. We formulated the design of 3D optimal solar-powered AUV trajectory as an optimization problem to maximize the harvested energy while minimizing its energy consumption. The optimization problem was numerically solved under data rate constraints imposed by the VLC link and in the presence of ocean currents. We investigated the amount of harvested power levels and consumed power levels as well as the net energy remaining in the battery for the optimal case as well as a benchmarking case where the solar-powered AUV swims at a fixed depth and the selection of sequence order of sensor nodes to be visited is not optimal. In the benchmarking case, it was observed that the AUV runs out of battery before the mission is complete resulting in a failure of autonomous operation. The results of the proposed EH-aware optimum trajectory demonstrated that the autonomous operation can last for longer durations without the need for the AUV to go back to the home base for recharging its batteries.

Appendix I

When the AUV is on the surface, the solar intensity normal to the panel's surface is dependent on the panel tilt (Ω) and solar zenith angle (ς), i.e., the angle between the sun's rays and the vertical direction, as shown in Fig.3. b. In an underwater scenario, it can be assumed that all of the solar intensity is vertical [40]. The amount of total intensity right before entering the water $\Psi_{0,\text{air}}[n]$ can be obtained by [48]

$$\Psi_{0,\text{air}}[n] = \Psi\left(1 + 0.033\cos\frac{360\Theta}{365}\right).\tau.\cos\left(\varsigma[n]\right), \quad (21)$$

where Ψ is the solar constant and Θ is the specific day of the year. Here, $\tau = 0.6174$ [48] is the atmospheric transmittance. In (21), ς is the solar zenith angle and is calculated as

$$\varsigma[n] = 90^\circ - \left[\sin^{-1}\left(\sin\left(\vartheta[n]\right)\sin\left(\delta\right) + \cos\left(\vartheta[n]\right)\cos\left(\delta\right)\cos\left(O\right)\right)\right], \quad (22)$$

where $\vartheta[n]$ is the latitude of the location of interest at time slot n. Here, δ denotes the solar declination (i.e., the angle between sun light's rays and the earth's equator) and is calculated as

$$\delta = 23.45\sin\left(360\frac{(248+\Theta)}{365}\right). \quad (23)$$

In (22), O is the hour angle (i.e., the number of degrees in which the sun moves across the sky) and calculated as

$$O[n] = \frac{(U[n] - 720)}{5}, \quad (24)$$

where U is the solar time (i.e., the local time based on the position of the sun in the sky). It is calculated as

$$U[n] = 60w + [4\left(l - \theta[n]\right) + E], \quad (25)$$

where w is hour of the day, l is the local standard time meridian for the time zone of the location of interest, and $\theta[n]$ is the longitude of the location of interest at time slot n. In (25), E is the equation of time which represents the difference between clock time and solar time and is given by

$$E = 9.87\sin\left(2\gamma\right) - 7.53\cos\left(\gamma\right) - 1.5\sin\left(\gamma\right), \quad (26)$$

where $\gamma = 360\left(\Theta + 81\right)/365$.

APPENDIX II

Let $\mathbf{b}$ denote a matrix containing the information on the sequence order of sensor nodes to be visited. It is given by

$$\mathbf{b} = \begin{pmatrix} b_{11} & \cdots & b_{1j} & \cdots & b_{1F} \\ \vdots & \vdots & \vdots & \vdots & \vdots \\ b_{i1} & \cdots & b_{ij} & \cdots & b_{iF} \\ \vdots & \vdots & \vdots & \vdots & \vdots \\ b_{F1} & \cdots & b_{Fj} & \cdots & b_{FF} \end{pmatrix}_{F\times F}, \quad (27)$$

where b_{ij} is set as 1 when the there is a path between sensor S_i to sensor S_j, and set as $b_{ij} = 0$ otherwise. As an example, to obtain components of $\mathbf{S}$, (i.e., $\mathrm{S}_{k,i}$, $k = 1, 2, ..., F$, $i = 1, 2, ..., F$), we sort the non-zero entries of matrix $\mathbf{b}$ as follows

$$\mathbf{b} = \begin{pmatrix} 0 & 1 & 0 & \cdots & 0 & 0 \\ 0 & 0 & 0 & \cdots & 1 & 0 \\ \vdots & \vdots & \vdots & \vdots & \vdots & \vdots \\ 0 & 0 & 0 & \ldots & 0 & 1 \\ 0 & 0 & 1 & \cdots & 0 & 0 \end{pmatrix}_{F\times F}$$

From the information given in the matrix $\mathbf{b}$, we extract the sequence order of nodes to be visited as $\mathbf{S} = (\mathrm{S}_{1,1}, \mathrm{S}_{2,2}, \mathrm{S}_{3,F-1}, ..., \mathrm{S}_{F-1,F}, \mathrm{S}_{F,3}$. For instance, $b_{12} = 1$ means that the AUV's optimum route is from sensor S_1 to the sensor S_2 ($\mathrm{S}_{1,1} \rightarrow \mathrm{S}_{2,2}$) and, $b_{2F-1} = 1$ means the AUV should go from sensor S_2 to the sensor S_{F-1} ($\mathrm{S}_{2,2} \rightarrow \mathrm{S}_{3,F-1}$) and so on.

REFERENCES

[1] K. K. Gola and B. Gupta, "Underwater sensor networks:'comparative analysis on applications, deployment and routing techniques'," *IET Communications*, vol. 14, no. 17, pp. 2859–2870, 2020.

[2] C. Christopoulou, H. G. Sandalidis, and I. S. Ansari, "Outage probability of a multisensor mixed uowc–fso setup," *IEEE Sensors Letters*, vol. 3, no. 8, pp. 1–4, 2019.

[3] H. Lei, Y. Zhang, K.-H. Park, I. S. Ansari, G. Pan, and M.-S. Alouini, "Performance analysis of dual-hop rf-uwoc systems," *IEEE Photonics Journal*, vol. 12, no. 2, pp. 1–15, 2020.

[4] P. Agheli, H. Beyranvand, and M. J. Emadi, "Uav-assisted underwater sensor networks using rf and optical wireless links," *Journal of Lightwave Technology*, vol. 39, no. 22, pp. 7070–7082, 2021.

[5] S. Li, L. Yang, D. B. da Costa, and S. Yu, "Performance analysis of uav-based mixed rf-uwoc transmission systems," *IEEE Transactions on Communications*, vol. 69, no. 8, pp. 5559–5572, 2021.

[6] J. Ren, Y. Zhang, K. Zhang, A. Liu, J. Chen, and X. S. Shen, "Lifetime and energy hole evolution analysis in data-gathering wireless sensor networks," *IEEE Transactions on Industrial Informatics*, vol. 12, no. 2, pp. 788–800, 2016.

[7] Y.-N. Ma, Y.-J. Gong, C.-F. Xiao, Y. Gao, and J. Zhang, "Path planning for autonomous underwater vehicles: An ant colony algorithm incorporating alarm pheromone," *IEEE Transactions on Vehicular Technology*, vol. 68, no. 1, pp. 141–154, 2019.

[8] R. Su, D. Zhang, C. Li, Z. Gong, R. Venkatesan, and F. Jiang, "Localization and data collection in auv-aided underwater sensor networks: Challenges and opportunities," *IEEE Network*, vol. 33, no. 6, pp. 86–93, 2019.

[9] E. M. Sozer, M. Stojanovic, and J. G. Proakis, "Underwater acoustic networks," *IEEE journal of oceanic engineering*, vol. 25, no. 1, pp. 72–83, 2000.

[10] A. Celik, N. Saeed, B. Shihada, T. Y. Al-Naffouri, and M.-S. Alouini, "End-to-end performance analysis of underwater optical wireless relaying and routing techniques under location uncertainty," *IEEE Transactions on Wireless Communications*, vol. 19, no. 2, pp. 1167–1181, 2020.

[11] M. F. Ali, D. N. K. Jayakody, and Y. Li, "Recent trends in underwater visible light communication (uvlc) systems," *IEEE Access*, vol. 10, pp. 22 169–22 225, 2022.

[12] P. A. Hoeher, J. Sticklus, and A. Harlakin, "Underwater optical wireless communications in swarm robotics: A tutorial," *IEEE Communications Surveys Tutorials*, vol. 23, no. 4, pp. 2630–2659, 2021.

[13] X. Sun, C. H. Kang, M. Kong, O. Alkhazragi, Y. Guo, M. Ouhssain, Y. Weng, B. H. Jones, T. K. Ng, and B. S. Ooi, "A review on practical considerations and solutions in underwater wireless optical communication," *Journal of Lightwave Technology*, vol. 38, no. 2, pp. 421–431, 2020.

[14] J. G. Bellingham, *Platforms: autonomous underwater vehicles*. San DIego, CA: Academic Press, 2008, vol. 6. [Online]. Available: http://dx.doi.org/10.1016/B978-012374473-9.00730-X

[15] J.-M. Tung, M.-F. Guo, J. Guo, F.-C. Chiu, and S.-W. Cheng, "Design of an underwater glider with fore and aft buoyancy engines," in *2007 Symposium on Underwater Technology and Workshop on Scientific Use of Submarine Cables and Related Technologies*. IEEE, 2007, pp. 446–450.

[16] J. Cao, D. Lu, D. Li, Z. Zeng, B. Yao, and L. Lian, "Smartfloat: A multimodal underwater vehicle combining float and glider capabilities," *IEEE Access*, vol. 7, pp. 77 825–77 838, 2019.

[17] A. A. R. Al Makdah, N. Daher, D. Asmar, and E. Shammas, "Three-dimensional trajectory tracking of a hybrid autonomous underwater vehicle in the presence of underwater current," *Ocean Engineering*, vol. 185, pp. 115–132, 2019.

[18] H. Nam, "Data-gathering protocol-based auv path-planning for long-duration cooperation in underwater acoustic sensor networks," *IEEE sensors journal*, vol. 18, no. 21, pp. 8902–8912, 2018.

[19] N. Javaid, N. Ilyas, A. Ahmad, N. Alrajeh, U. Qasim, Z. A. Khan, T. Liaqat, and M. I. Khan, "An efficient data-gathering routing protocol for underwater wireless sensor networks," *Sensors*, vol. 15, no. 11, pp. 29 149–29 181, 2015.

[20] A. Ahmad, A. Wahid, and D. Kim, "Aeerp: Auv aided energy efficient routing protocol for underwater acoustic sensor network," in *Proceedings of the 8th ACM workshop on Performance monitoring and measurement of heterogeneous wireless and wired networks*, 2013, pp. 53–60.

[21] N. Wang and J. Wu, "Trajectory scheduling for timely data report in underwater wireless sensor networks," in *2015 IEEE Global Communications Conference (GLOBECOM)*. IEEE, 2015, pp. 1–6.

[22] N. Ilyas, N. Javaid, Z. Iqbal, M. Imran, Z. A. Khan, U. Qasim, and M. Shoaib, "Aaeerp: Advanced auv-aided energy efficient routing protocol for underwater wsns," in *2015 IEEE 29th International Conference on Advanced Information Networking and Applications*. IEEE, 2015, pp. 77–83.

[23] X. Zhuo, M. Liu, Y. Wei, G. Yu, F. Qu, and R. Sun, "Auv-aided energy-efficient data collection in underwater acoustic sensor networks," *IEEE Internet of Things Journal*, vol. 7, no. 10, pp. 10 010–10 022, 2020.

[24] C. Qin, J. Du, J. Wang, and Y. Ren, "A hierarchical information acquisition system for auv assisted internet of underwater things," *IEEE Access*, vol. 8, pp. 176 089–176 100, 2020.

[25] F. A. Khan, S. A. Khan, D. Turgut, and L. Bölöni, "Scheduling multiple mobile sinks in underwater sensor networks," in *2015 IEEE 40th Conference on Local Computer Networks (LCN)*. IEEE, 2015, pp. 149–156.

[26] G. A. Hollinger, S. Choudhary, P. Qarabaqi, C. Murphy, U. Mitra, G. S. Sukhatme, M. Stojanovic, H. Singh, and F. Hover, "Underwater data collection using robotic sensor networks," *IEEE Journal on Selected Areas in Communications*, vol. 30, no. 5, pp. 899–911, 2012.

[27] P. Gjanci, C. Petrioli, S. Basagni, C. A. Phillips, L. Bölöni, and D. Turgut, "Path finding for maximum value of information in multi-modal underwater wireless sensor networks," *IEEE Transactions on Mobile Computing*, vol. 17, no. 2, pp. 404–418, 2017.

[28] K. A. Mahmoodi and M. Uysal, "Auv trajectory optimization for an optical underwater sensor network in the presence of ocean currents," in *2021 IEEE International Black Sea Conference on Communications and Networking (BlackSeaCom)*. IEEE, 2021, pp. 1–6.

[29] D. R. Blidberg, S. Chappell, and J. C. Jalbert, "Long endurance sampling of the ocean with solar powered auv's," *IFAC Proceedings Volumes*, vol. 37, no. 8, pp. 561–566, 2004.

[30] D. M. Crimmins, C. T. Patty, M. A. Beliard, J. Baker, J. C. Jalbert, R. J. Komerska, S. G. Chappell, and D. R. Blidberg, "Long-endurance test results of the solar-powered auv system," in *OCEANS 2006*. IEEE, 2006, pp. 1–5.

[31] P. P. Jenkins, S. Messenger, K. M. Trautz, S. I. Maximenko, D. Goldstein, D. Scheiman, R. Hoheisel, and R. J. Walters, "High-bandgap solar cells for underwater photovoltaic applications," *IEEE Journal of Photovoltaics*, vol. 4, no. 1, pp. 202–207, 2013.

[32] https://www.evologics.de/en/products/lbl/index.html.

[33] https://www.km.kongsberg.com/ks/web/nokbg0240.nsf.

[34] Y. Weng, T. Matsuda, Y. Sekimori, J. Pajarinen, J. Peters, and T. Maki, "Pointing error control of underwater wireless optical communication on mobile platform," *IEEE Photonics Technology Letters*, vol. 34, no. 13, pp. 699–702, 2022.
[35] X. Yao, F. Wang, J. Wang, and X. Wang, "Bilevel optimization-based time-optimal path planning for auvs," *Sensors*, vol. 18, no. 12, p. 4167, 2018.
[36] M. E. Furlong, S. D. McPhail, and P. Stevenson, "A concept design for an ultra-long-range survey class auv," in *OCEANS 2007-Europe*. IEEE, 2007, pp. 1–6.
[37] Y. Song, H. Ye, Y. Wang, W. Niu, X. Wan, and W. Ma, "Energy consumption modeling for underwater gliders considering ocean currents and seawater density variation," *Journal of Marine Science and Engineering*, vol. 9, no. 11, 2021. [Online]. Available: https://www.mdpi.com/2077-1312/9/11/1164
[38] A. Phillips, M. Haroutunian, A. J. Murphy, S. Boyd, J. Blake, and G. Griffiths, "Understanding the power requirements of autonomous underwater systems, part i: An analytical model for optimum swimming speeds and cost of transport," *Ocean Engineering*, vol. 133, pp. 271–279, 2017.
[39] M. Paulescu, E. Paulescu, P. Gravila, and V. Badescu, *Modeling Solar Radiation at the Earth Surface*. London: Springer London, 2013, pp. 127–179. [Online]. Available: https://doi.org/10.1007/978-1-4471-4649-0_5
[40] G. G. Hahn, L. A. Adoram-Kershner, H. P. Cantin, and M. W. Shafer, "Assessing solar power for globally migrating marine and submarine systems," *IEEE Journal of Oceanic Engineering*, vol. 44, no. 3, pp. 693–706, 2018.
[41] J. Lin, Z. Du, C. Yu, W. Ge, W. Lü, H. Deng, C. Zhang, X. Chen, Z. Zhang, and J. Xu, "Machine-vision-based acquisition, pointing, and tracking system for underwater wireless optical communications," *Chin. Opt. Lett.*, vol. 19, no. 5, p. 050604, May 2021. [Online]. Available: http://opg.optica.org/col/abstract.cfm?URI=col-19-5-050604
[42] R. Jiang, Z. Wang, Q. Wang, and L. Dai, "A tight upper bound on channel capacity for visible light communications," *IEEE Communications Letters*, vol. 20, no. 1, pp. 97–100, 2015.
[43] C. D. Mobley, B. Gentili, H. R. Gordon, Z. Jin, G. W. Kattawar, A. Morel, P. Reinersman, K. Stamnes, and R. H. Stavn, "Comparison of numerical models for computing underwater light fields," *Applied Optics*, vol. 32, no. 36, pp. 7484–7504, 1993.
[44] J. Stastnỳ, V. Skorpil, and L. Cizek, "Traveling salesman problem optimization by means of graph-based algorithm," in *2016 39th International Conference on Telecommunications and Signal Processing (TSP)*. IEEE, 2016, pp. 207–210.
[45] Z. Zeng, A. Lammas, K. Sammut, and F. He, "Optimal path planning based on annular space decomposition for auvs operating in a variable environment," in *2012 IEEE/OES Autonomous Underwater Vehicles (AUV)*. IEEE, 2012, pp. 1–9.
[46] L. Wang, L. Liu, J. Qi, and W. Peng, "Improved quantum particle swarm optimization algorithm for offline path planning in auvs," *IEEE Access*, vol. 8, pp. 143 397–143 411, 2020.
[47] D. Corus and P. S. Oliveto, "Standard steady state genetic algorithms can hillclimb faster than mutation-only evolutionary algorithms," *IEEE Transactions on Evolutionary Computation*, vol. 22, no. 5, pp. 720–732, 2017.
[48] J.-S. Lee and K.-H. Yu, "Optimal path planning of solar-powered uav using gravitational potential energy," *IEEE Transactions on Aerospace and Electronic Systems*, vol. 53, no. 3, pp. 1442–1451, 2017.
[49] J. Heidemann, W. Ye, J. Wills, A. Syed, and Y. Li, "Research challenges and applications for underwater sensor networking," in *IEEE Wireless Communications and Networking Conference, 2006. WCNC 2006.*, vol. 1, 2006, pp. 228–235.
[50] http://www.teledynemarine.com/gavia-auv?brandid=9.
[51] M. Arima, T. Okashima, and T. Yamada, "Development of a solar-powered underwater glider," in *2011 IEEE Symposium on Underwater Technology and Workshop on Scientific Use of Submarine Cables and Related Technologies*, 2011, pp. 1–5.

Khadijeh Ali Mahmoodi received her B.Sc. degree in electrical and electronics engineering from Tafresh University, Tafresh, Iran, in 2015. She joined Optoelectronics and Optical Communications Research Laboratory (OOCRL) research center in 2016 working toward her M.Sc. degree in electrical and electronics engineering at Isfahan University of Technology, Isfahan, Iran, and completed her M.Sc. in 2019. She joined the Communication Theory and Technologies (CT&T) Research Group in 2020 and has been pursuing her Ph.D. under the supervision of Prof. Murat Uysal at Özyeğin University, Istanbul, Turkiye.

She is also a member of ENLIGHTEM project working as a Marie Curie Early-Stage Researcher. Her research interests include low energy visible light communication systems, underwater sensor networks, energy harvesting, trajectory optimization of autonomous underwater vehicles (AUVs) and unmanned aerial vehicles (UAVs) in communication networks.

Murat Uysal received the B.Sc. and the M.Sc. degree in electronics and communication engineering from Istanbul Technical University, Istanbul, Turkiye, in 1995 and 1998, respectively, and the Ph.D. degree in electrical engineering from Texas A&M University, College Station, Texas, in 2001. He is currently a Full Professor and Chair of the Department of Electrical and Electronics Engineering at Ozyegin University, Istanbul, Turkey. He also serves as the Founding Director of the Center of Excellence in Optical Wireless Communicaion Technologies (OKATEM). Prior to joining Ozyegin University, he was a tenured Associate Professor at the University of Waterloo, Canada. Dr. Uysal's research interests are in the broad area of communication theory with a particular emphasis on the physical layer aspects of wireless communication systems in radio and optical frequency bands. On these topics, he has authored some 350 journal and conference papers and received more than 13.000 citations with an h-index of 56.

Dr. Uysal is an IEEE Fellow and the former Chair of IEEE Turkey Section. He currently serves on the editorial board of IEEE Transactions on Wireless Communications. In the past, he served as an Editor for IEEE Transactions on Communications, IEEE Transactions on Vehicular Technology, and IEEE Communications Letters. He was involved in the organization of several IEEE conferences at various levels. In particular, he served as the Technical Program Committee Chair of major IEEE conferences including WCNC 2014, PIMRC 2019 and VTC-Fall 2019.

Prof Uysal's major distinctions include NSERC Discovery Accelerator Award in 2008, University of Waterloo Engineering Research Excellence Award in 2010, Turkish Academy of Sciences Distinguished Young Scientist Award in 2011, Ozyegin University Best Researcher Award in 2014, National Instruments Engineering Impact Award in 2017, Elginkan Foundation Technology Award in 2018 and IEEE Communications Society Best Survey Paper Award in 2019 among others.